Axial superresolution by synthetic aperture generation

2008 J. Opt. A: Pure Appl. Opt. 10 125001

(http://iopscience.iop.org/1464-4258/10/12/125001)

J. Opt. A: Pure Appl. Opt. **10** (2008) 125001 (8pp) doi:10.1088/1464-4258/10/12/125001

Axial superresolution by synthetic aperture generation

V Micó[1], J García[1] and Z Zalevsky[2]

[1] Departamento de Óptica, Universitat de València, C/ Dr. Moliner, 50, 46100 Burjassot, Spain
[2] School of Engineering, Bar-Ilan University, Ramat-Gan, 52900, Israel

E-mail: Vicente.Mico@uv.es

Received 19 July 2008, accepted for publication 30 September 2008
Published 31 October 2008
Online at stacks.iop.org/JOptA/10/125001

Abstract
The use of tilted illumination onto the input object in combination with time multiplexing is a useful technique to overcome the Abbe diffraction limit in imaging systems. It is based on the generation of an expanded synthetic aperture that improves the cutoff frequency (and thus the resolution limit) of the imaging system. In this paper we present an experimental validation of the fact that the generation of a synthetic aperture improves not only the lateral resolution but also the axial one. Thus, it is possible to achieve higher optical sectioning of three-dimensional (3D) objects than that defined by the theoretical resolution limit imposed by diffraction. Experimental results are provided for two different cases: a synthetic object (micrometer slide) imaged by a 0.14 numerical aperture (NA) microscope lens, and a biosample (swine sperm cells) imaged by a 0.42 NA objective.

Keywords: digital holographic microscopy, synthetic aperture microscopy, Fourier image formation, superresolution, optical sectioning

(Some figures in this article are in colour only in the electronic version)

1. Introduction

Optical superresolution is a handy field proposed mainly to overcome the Abbe diffraction limit in imaging systems [1]. The first attempts in experimental validation on superresolution imaging were proposed by Lukosz *et al* [2–5]. Lukosz [3, 4] laid the foundations of optical superresolution by means of the definition of an invariance theorem that states that is not the spatial bandwidth but the number of degrees of freedom of the system that is constant. Using this invariance theorem, Lukosz theorized that any parameter in the system could be extended above the classical limit if any other factor is proportionally reduced, provided that some *a priori* information concerning the object is known. Thus, it is in principle possible to extend the spatial bandwidth by encoding–decoding an additional object's spatial-frequency information onto the independent (unused) parameters of the imaging system. *A priori* knowledge permits the classification of objects into different types and allows different superresolution strategies depending on such classification: time multiplexing for temporally restricted objects [3, 6], spectral encoding in wavelength restricted objects [7–9], spatial multiplexing for one-dimensional objects [10, 11], polarization coding with polarization restricted objects [12, 13], and gray level coding for objects with restricted intensity dynamic range [14].

One of the most appealing approaches concerning the superresolution effect is presented when the objects are statics or have slow variation in time [15]. Superresolution with temporally restricted objects can be achieved by time multiplexing the spatial-frequency bandwidth of the object in such a way that different frequency band passes are transmitted through the limited system aperture in different time slots. Then, considering a full multiplexing cycle, it is possible to improve the resolution of the imaging system in terms of the definition of an expanded synthetic aperture that provides a wider coverage of the 2D object's spectrum in comparison with the conventional case. Several approaches exhibiting transversal superresolution imaging have been proposed through the years in different application fields such as lithography [16–19], fluorescent microscopy [20–23], scanning holographic microscopy [24, 25], imaging through a turbid medium [26–28], and digital holographic microscopy [29–33]. The underlying principle of all of these approaches is to illuminate the object with a set of tilted beams or to project a grid pattern onto it.

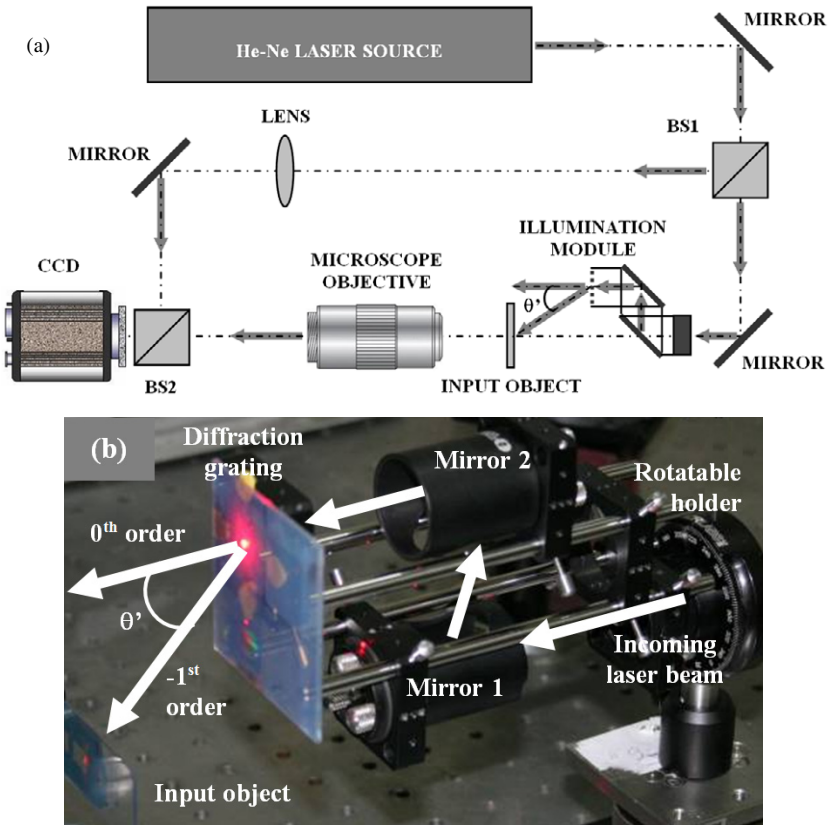

Figure 1. (a) The experimental setup used in the proposed approach and (b) a picture of the illumination module. In both cases, gray and white arrows depict the optical beam path of the laser light.

Then, by time multiplexing several object orientations, it is possible to define a synthetic numerical aperture with improved cutoff frequency and, thus, with improved spatial resolution.

But the generation of such an expanded synthetic aperture not only improves the lateral resolution. Since the axial extent of the focal spot is proportional to NA^{-2} [34], a synthetic widening in the NA also implies a non-linear improvement in the axial resolution. This is of particular importance in microscopy where high optical sectioning with high transversal resolution while maintaining a large field of view and large working distance is of practical interest in many applications in life science [35–39]. Because low to medium NA lenses (ranging from 0.1 to 0.5 in NA value) are the most commonly used lenses in microscopy applications, the axial resolution provided by these lenses is dramatically poorer than the transversal resolution because of the non-linear proportion. Due to its practical benefits, different approaches have been proposed over the years to overcome this [40–44]. In this paper, we experimentally show that synthetic numerical aperture generation using tilted beams provides full (transversal and axial) superresolution imaging. As a first case, the obtained experimental results are in good agreement with theoretical predictions when a low NA microscope lens (0.14 NA) images a synthetic object. After that, a second experimental case is presented in which a medium NA lens (0.42 NA) is used to image a biosample. We will first introduce the proposed methodology and then we will present its experimental validation.

2. Methodology

The optical system setup used in the experimental validation of the proposed approach is depicted in figure 1(a). A first beam splitter (BS1) allows the implementation of a Mach–Zehnder interferometric architecture by splitting the incoming light beam from a He–Ne laser into two beams. On one branch (the imaging branch), we assemble a microscope configuration in transmission mode; a microscope objective magnifies a transparent object onto a CCD.

Two different cases are considered. In the first one (named the one-dimensional (1D) case), the input object is mounted obliquely at the input plane by tilting it around the vertical axis. The tilt in the input object is properly adjusted to bring the image out of focus at its borders while remaining in focus at its central part. Thus, only a narrow zone of the input object is imaged in focus. This case will be used to quantify axial resolution and compare experimental value with theoretical predictions. In the second case (named the two-dimensional (2D) case), the object is not tilted at the input plane but it is not imaged at the CCD; that is, no particular object plane is imaged in focus at the CCD plane. This effect can be achieved by either moving the CCD back or moving the input sample forward. Thus, the CCD images a magnified wavefront coming from the image plane but not a focused image of the object itself.

Then, by adding a reference beam incoming from the second branch (the reference branch) of the interferometric configuration, the CCD records a hologram of the transmitted

object wavefront. In the 1D case, the recorded hologram will be an image plane hologram, while in the 2D case it will be a Fresnel hologram of the object wavefront transmitted through the aperture lens. But because the bending mirror of the reference branch is slightly tilted, the reference beam reaches the CCD at oblique incidence; that is, an off-axis holographic recording geometry is produced. This allows access to the transmitted spatial-frequency band-pass through the microscope limited aperture by simple Fourier transformation of the recorded hologram. Moreover, as the presence of a lens in the reference branch allows divergence compensation between both interferometric beams, the recovered frequency band does not suffer from misfocus during the recording process.

In this digital holographic microscope configuration and considering on-axis conventional illumination, the object imaged at the CCD will be limited in both transversal and axial resolution according to the theory; that is, λ/NA and λ/NA^2 respectively, where λ is the illumination wavelength. Notice that no geometrical constraints are considered regarding the pixel size of the CCD (no geometrical resolution limit is produced) because the magnification that is achieved at the image plane is high enough to avoid aliasing problems.

Now, oblique illumination is sequentially applied on the input object by the action of an illumination module placed on a rotatable holder and composed of two mirrors with a 45° configuration and a 1D diffraction grating. A picture of such an assembly is presented in figure 1(b). The mirrors shift the incoming laser beam parallel to the optical axis and oblique illumination is produced onto the input plane by considering the -1 diffraction order of the grating. If the basic frequency of the grating is chosen to diffract light at an angle θ' that is close to double the angle defined by the NA of the microscope lens, a quasi-continuous spatial-frequency band of the input object's spectrum will be diffracted on-axis passing though the limited aperture of the lens (see [32]). Posterior off-axis holographic recording allows the recovery of each elementary pupil using digital post-processing that involves simple numerical manipulation operations (filtering and centering of each recovered pupil) and that allows the generation of the expanded synthetic aperture.

With this illumination assembly, different oblique illuminations can be performed in sequential mode by rotating the mount that holds the illumination module around the optical axis. In addition, on-axis illumination is also considered by removing the illumination module. In order to expand the imaging system aperture, only horizontal illumination is considered in the 1D case (only two positions of the illumination module) while a set of eight positions is needed to fully expand the aperture in the 2D case and achieve a 2D frequency space coverage (eight positions with a 45° step between them). In both cases, the synthetic aperture will be composed by the sequential addition of different elementary pupils, each one corresponding to different tilted illumination onto the input object. Thus, the generated synthetic aperture expands up the cutoff frequency of the microscope lens for every considered direction and according to $f'_{\mathrm{cutoff}} = \mathrm{SNA}/\lambda$ [16–19, 29–33], where $\mathrm{SNA} = \mathrm{NA} + \mathrm{NA}_{\mathrm{ilum}}$ is the synthetic numerical aperture after applying time multiplexing with tilted beams, and $\mathrm{NA}_{\mathrm{ilum}}$ is the NA of the tilted illumination ($\mathrm{NA}_{\mathrm{ilum}} = \sin\theta'$).

This SNA definition makes the proposed system (microscope lens with the time multiplexing approach using tilted beams) and a microscope objective with an NA equal to the SNA that has been generated completely equivalent. As a consequence, the transversal and axial resolutions are redefined according to λ/SNA and λ/SNA^2, respectively.

3. Experimental validation

In this section we present the experimental results obtained using the proposed approach, separated into two cases. In the first, a 1D validation with quantitative values is presented when a 0.14 NA microscope lens images a 1D micrometer slide. The axial resolution measured is in concordance with the theoretically predicted one once a 1D synthetic aperture is generated. In the second case, we show a qualitative 2D implementation with a swine sperm sample as an object to be imaged by a 0.42 NA microscope objective. Thus, the sequence of images obtained by refocusing the sample at different planes will evidence the improvement in both transversal and axial resolution obtained by using the proposed approach. In both cases, a He–Ne laser source (0.6328 μm wavelength) and Kappa DC2 camera (12 bits, 1352 × 1014 pixels with 6.7 μm pixel size) are used as illumination light and CCD, respectively.

A common procedure can be defined for the two proposed cases. A set of different off-axis holograms corresponding to each illumination beam (on-axis and off-axis light beams) is stored in the memory of the computer. Then, the complex amplitude distribution of each transmitted frequency band-pass is recovered by applying a Fourier transformation over each recorded hologram and considering the distribution located at one of the diffraction orders. After the filtering and centering process, each recovered elementary pupil is properly replaced at its original position of the object's spectrum, allowing the generation of the synthetic aperture by sequential addition of the different single pupils. Finally, a superresolved image is obtained by Fourier transformation of the information contained in the generated synthetic aperture.

3.1. 1D case: synthetic objects

Although other more complicated methods can be used, the axial resolution of a microscope lens can be measured quickly and unambiguously using the image provided by the lens itself and a particular assembly at the input plane. When a given periodic structure is mounted obliquely at the input plane and imaged by a lens, only a narrow area of such a structure will appear in focus. Thus, the axial resolution can be calculated from the width of the focused area (directly measured in the image), the refractive index of the medium surrounding the structure (air in our case), and the rotation angle of the structure (a known value).

In our case, we use a micrometer slide as the input structure and a 0.14 NA Mitutoyo infinity corrected long

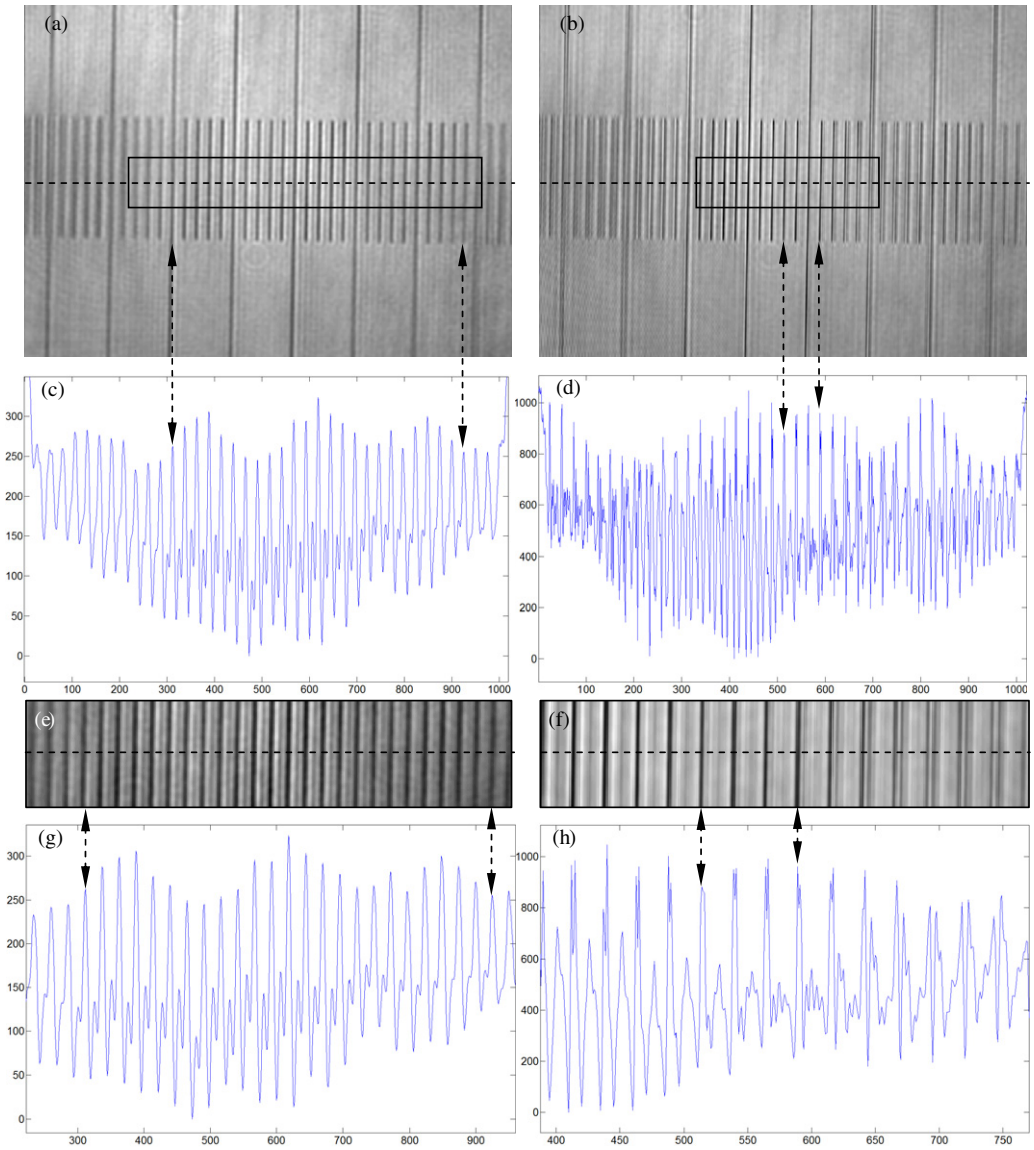

Figure 2. Experimental results when a micrometer slide is imaged by a 0.14 NA lens without (left column) and with (right column) consideration of the proposed approach. Black dashed arrows mark the edge lines considered to determine the focused intervals. Cases (c) and (d) represent a plot along the black dashed line in cases (a) and (b), respectively. Cases (e) and (f) image the magnified area marked with the solid black rectangle in cases (a) and (b), respectively, and cases (g) and (h) plot the black dashed line in cases (e) and (f), respectively.

working distance microscope objective as the imaging lens. The image sequence corresponding to the 1D case is depicted in figure 2. The stage micrometer is a clear glass slide with black anodized aluminum lines having a separation of 10 μm between two consecutive lines. The micrometer slide is tilted 8° at the input plane to bring the lines at the borders of the image out of focus (figure 2(a)). According to the theoretical calculations, the axial resolution provided by the lens is 32.3 μm. As we will see, this value is in good agreement with the measured one, where 24 lines (240 μm) are in focus, which means an axial resolution value of approximately 33 μm when considering the object's tilt.

To calculate the axial resolution value experimentally, we define a criterion based on image analysis taking into account the following procedure. We plot a section of the image depicted in figure 2(a) along its black dashed horizontal line. The result is depicted in figure 2(c) and magnified in figure 2(g). As edge lines of the focused interval we have chosen the ones from which the second peak of each line disappears. This second peak has a lower intensity because it is originated from a double image incoming from the reflection between the two sides of the micrometer slide. This double image can be clearly seen from the picture shown in figure 2(e). So, when this double image mixes with the direct one, we consider that the image is blurred. This criterion is reinforced by visual comparison through the image presented in figure 2(a), where the lines that are selected in figures 2(e) and (g) using the previous criterion are the same ones that one may select visually.

Now, we perform the superresolution approach when only two tilted beams in the horizontal direction are considered. The oblique illumination is produced by impinging onto the

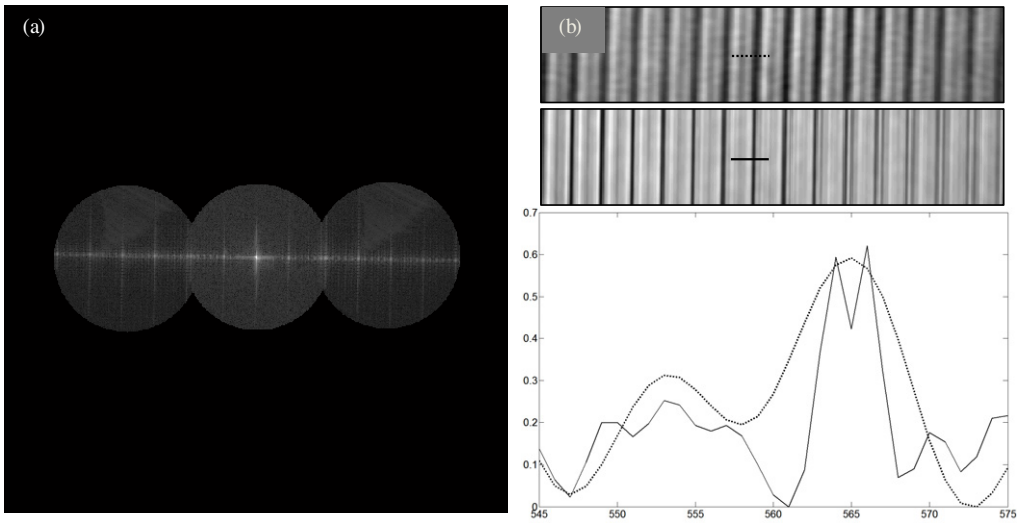

Figure 3. (a) Generated synthetic aperture for the 1D case and (b) comparison of transversal resolution between the same focused line (the central one of the in-focus interval) by taking the proposed approach into account (solid case) or not (dotted case).

micrometer slide the -1 diffraction order of a 1D Ronchi ruling grating with 400 lp mm^{-1} (2.5 μm) basic period. According to the grating equation, the off-axis illumination angle is approximately 14.7°, and the generated synthetic aperture has a value of 0.39 SNA in the horizontal direction.

To calculate the new interval of focused lines, we have plotted again a profile along the same black dashed line as in the previous case. The result is depicted in figure 2(d), while a magnification of the focused area is depicted in figure 2(f) and plotted in case (h). Now, we have selected the interval of lines where the double image minimizes its intensity. Because the blur first affects the high spatial-frequency content rather than the low one, we have chosen as the interval of focused lines the interval which minimizes the intensity of the background between lines. Thus, three lines compose the focused interval, which implies an axial resolution of approximately 4 μm. This value is again in agreement with the theoretical value that is obtained from the SNA value, that is, 4.1 μm.

Figure 3(a) depicts the synthetic aperture generated when off-axis horizontal illumination is considered. We can see that two quasi-contiguous elementary pupils expand the cutoff frequency of the imaging system and allow a resolution gain factor that is close to 3 (in the horizontal direction) in comparison with the conventional imaging mode (central pupil in figure 3(a) corresponding to on-axis illumination). This can be clearly seen from figure 3(b), where a plot along the dotted and solid black lines highlight the improvement in transversal resolution. The represented plot depicts the central focused line of the in-focus interval for the low resolution (dotted case) and the superresolved (solid case) images. Note that the superresolved case makes the plotted line of the micrometer slide narrower in comparison with the low resolution image.

3.2. 2D case: swine sperm sample

A second experiment is presented considering a 2D superresolution effect and a swine sperm sample as input object. The unstained sample is enclosed in a counting chamber and it is dried, thus providing static sperm cells for the experiments. The sperm cells have a head dimension of 6 μm $\times$ 9 μm corresponding to the width and height of the ellipsoidal shape of the head, a total length of 55 μm, and a tail width of 2 μm on the head side and 1 μm at the end, approximately. The purpose of this experiment is to qualitatively demonstrate that the generation of a synthetic aperture by means of tilted beams and time multiplexing holography improves the optical sectioning capabilities, or in other words, the axial resolution, as well as the transversal one. To do this, the sample is not tilted at the input plane but the image onto the CCD is deliberately misfocused. This allows the posterior numerical refocusing of the recovered image at different arbitrary reconstruction distances. In other words, we are able to bring into focus different axial planes corresponding to different sections of the sample.

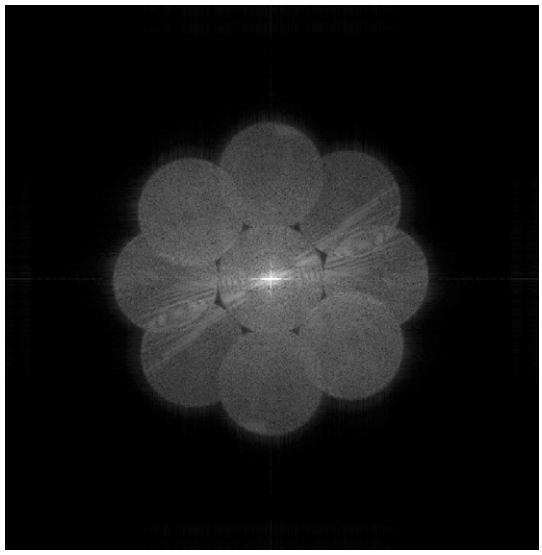

Figure 4. Generated synthetic aperture for the 2D case.

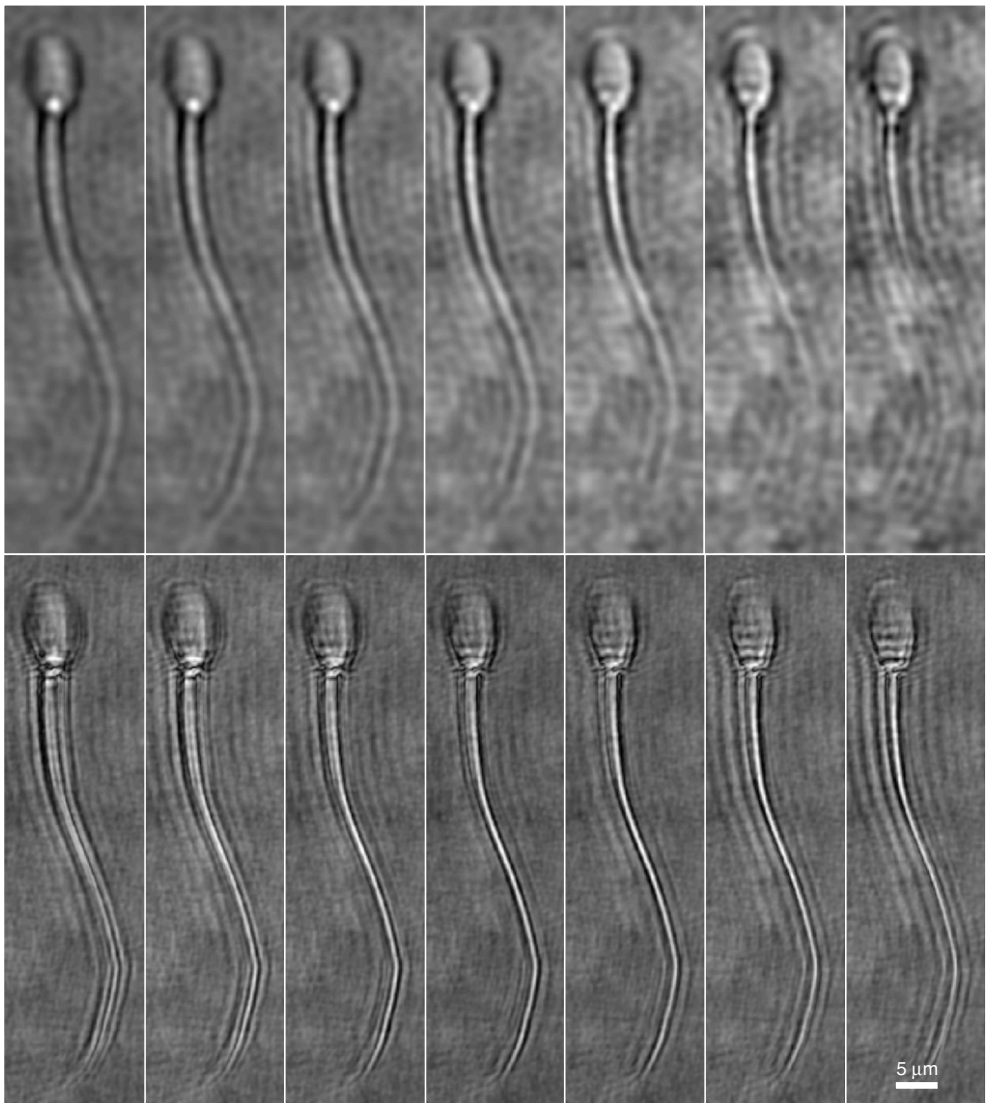

Figure 5. A set of refocused swine cell images at different axial distances without (upper row) and with (lower row) applying the proposed approach. Thus, every pair of images in each column corresponds to the same swine cell that is refocused at the same distance but taking into account (lower row) or not (upper row) the proposed approach.

The grating used in the illumination module (see figure 1(b)) is holographically recorded and it has a 1D period of 0.8 μm. Thus, the first-order beam is diffracted at an angle of 52° and it is used to illuminate the sample obliquely. The sample is imaged in a plane prior to the CCD by a 0.42 NA Mitutoyo infinity corrected long working distance microscope objective. Computational refocusing is performed using the convolution method, which states that the diffraction integral is calculated using three Fourier transformations through the convolution theorem. The numerical computation of the Fourier transformation operation is realized with the FFT algorithm.

In order to achieve 2D frequency space coverage of the object's spectrum, a set of nine illumination beams (one on-axis plus eight off-axis) is considered in a sequential mode. Each recorded hologram is stored in the memory of the computer and after applying the filtering and centering process in the diffracted order of the recorded hologram a numerical refocusing is performed in a posterior digital post-processing stage. This allows the definition of a synthetic aperture from the addition of the different elementary pupils for every propagation distance. Figure 4 depicts one such synthetic aperture. We can see that the SA is composed of one on-axis and eight off-axis pupils, allowing the improvement of the cutoff frequency to a value that is close to triple the conventional one. In addition, and according to the theoretical predictions, the SNA of the microscope lens using the proposed approach is expanded up to 1.20 SNA, approximately.

Figure 5 depicts a set of refocused images for different reconstruction distances. The upper row corresponds to the case of conventional imaging (0.42 NA lens and on-axis illumination) and the lower row depicts the case where the refocusing is performed considering the generated synthetic aperture. We can see that, besides the transversal resolution improvement clearly visible in each pair of upper and lower images, the axial resolution is very much improved. The

theoretical limits for the transversal and axial resolutions are 1.5 μm and 3.6 μm for the conventional imaging mode and 0.5 μm and 0.4 μm when using the proposed approach, respectively. We can see that the tail of the sperm cell, which is not visible under conventional illumination mode because it is below the diffraction limit of the microscope lens (upper row), now becomes resolved using the proposed approach (lower row). Moreover, as both the tail width and the head diameter of the swine sperm are smaller than the axial resolution limit in the conventional case, the sperm cell is practically invariant to the reconstruction distance and always appears in focus in any image presented in the upper row.

Due to the SNA definition, both the axial and transversal resolution limits are decreased, allowing optical sectioning of the sperm cell. We can see that the left image in the lower row has a circular shape in the cell head near the neck. This structure, which is placed in the upper side of the sperm head, is not present in the right image of the lower row that corresponds to the lower side of the sperm head. In fact, and according to the theoretical values, we have achieved an axial resolution which is lower than the transversal one; that is, the optical system has higher capabilities for optical sectioning than for conventional imaging. This is due to the non-linear proportion in the definition of the axial resolution limit.

4. Conclusions

In this paper we have demonstrated experimentally that synthetic aperture generation improves not only the transversal resolution but also the axial resolution. The synthetic aperture generation is based on a time multiplexing process composed of sequential illumination of tilted beams onto the input object, holographic recording of the transmitted wavefront for each tilted illumination, and digital manipulation of the set of recorded holograms. This whole process finally culminates with the definition of an expanded aperture that improves both the axial and transversal resolutions. Experimental validations are in good agreement with the theoretical predictions.

In a first experiment, off-axis image plane recording allows the recovery of each transmitted elementary pupil having different spatial information selected by the each tilted illumination beam. In a second experiment, non-image plane holographic recording allows numerical refocusing of different transversal planes of the sample in a later post-processing stage. Because of the coherent nature of the experiments, the range for focusing the image can be almost infinite, while the axial resolution becomes improved by synthetic aperture generation. Thus, it is possible to focus on different cross sections along the optical axis, allowing superresolution imaging of different sections of the input sample. This implies attractive advantages with respect to the incoherent illumination case, where the defocus means a loss in the spatial-frequency content of the object's spectrum and no refocusing in the reconstruction process can be performed.

Acknowledgments

The authors want to thank Professor Carles Soler and Paco Blasco from Proiser R+D S.L. for providing the swine sperm sample. Also, part of this work was supported by the Spanish Ministerio de Educación y Ciencia under the project FIS2007-60626.

References

[1] Abbe E 1873 Beitrage zur theorie des mikroskops und der mikroskopischen wahrnehmung *Arch. Mikrosk. Anat.* **9** 413–68
[2] Lukosz W and Marchand M 1963 Optischen abbildung unter überschreitung der beugungsbedingten auflösungsgrenze *Opt. Acta* **10** 241–55
[3] Lukosz W 1966 Optical systems with resolving powers exceeding the classical limits *J. Opt. Soc. Am.* **56** 1463–72
[4] Lukosz W 1967 Optical systems with resolving powers exceeding the classical limits II *J. Opt. Soc. Am.* **57** 932–41
[5] Bachl A and Lukosz W 1967 Experiments on superresolution imaging of a reduced object field *J. Opt. Soc. Am.* **57** 163–9
[6] Shemer A, Mendlovic D, Zalevsky Z, García J and García-Martínez P 1999 Superresolving optical system with time multiplexing and computer decoding *Appl. Opt.* **38** 7245–51
[7] Kartashev A I 1960 Optical systems with enhanced resolving power *Opt. Spectrosc.* **9** 204–6
[8] Armitage J D, Lohmann A W and Parish D P 1965 Superresolution image forming systems for objects with restricted lambda dependence *Japan. J. Appl. Phys.* **4** 273–5
[9] Alexandrov S A and Sampson D D 2008 Spatial information transmission beyond a system's diffraction limit using optical spectral encoding of the spatial frequency *J. Opt. A: Pure Appl. Opt.* **10** 025304
[10] Grim M A and Lohmann A W 1966 Super resolution image for 1D objects *J. Opt. Soc. Am.* **56** 1151–6
[11] Bartelt H and Lohmann A W 1982 Optical processing of 1D signals *Opt. Commun.* **42** 87–91
[12] Lohmann A W and Paris D 1964 Superresolution for nonbirefringent objects *J. Opt. Soc. Am.* **3** 1037–43
[13] Zlotnik A, Zalevsky Z and Marom E 2005 Superresolution with nonorthogonal polarization coding *Appl. Opt.* **44** 3705–15
[14] Zalevsky Z, García-Martínez P and García J 2006 Superresolution using gray level coding *Opt. Express* **14** 5178–82
[15] Zalevsky Z and Mendlovic D 2002 *Optical Super Resolution* (Berlin: Springer)
[16] Chen X and Brueck S R J 1999 Imaging interferometric lithography: approaching the resolution limits of optics *Opt. Lett.* **24** 124–6
[17] Schwarz C J, Kuznetsova Y and Brueck S R J 2003 Imaging interferometric microscopy *Opt. Lett.* **28** 1424–6
[18] Kuznetsova Y, Neumann A and Brueck S R J 2007 Imaging interferometric microscopy—approaching the linear systems limits of optical resolution *Opt. Express* **15** 6651–63
[19] Neumann A, Kuznetsova Y and Brueck S R J 2008 Structured illumination for the extension of imaging interferometric microscopy *Opt. Express* **16** 6785–93
[20] Gustafsson M G L 2000 Surpassing the lateral resolution limit by a factor of two using structured illumination microscopy *J. Microsc.* **198** 82–7
[21] Heintzmann R, Jovin T M and Cremer C 2002 Saturated patterned excitation microscopy—a concept for optical resolution improvement *J. Opt. Soc. Am.* A **19** 1599–609
[22] Heintzmann R and Benedetti P A 2006 high-resolution image reconstruction in fluorescence microscopy with patterned excitation *Appl. Opt.* **45** 5037–45
[23] Hell S W and Wichmann J 1994 Breaking the diffraction resolution limit the stimulated emission: stimulated emission depletion microscopy *Opt. Lett.* **19** 780–2
[24] Indebetouw G, El Maghnouji A and Foster R 2005 Scanning holographic microscopy with transverse resolution

exceeding the Rayleigh limit and extended depth of focus *J. Opt. Soc. Am.* A **22** 892–8
[25] Indebetouw G, Tada Y, Rosen J and Brooker G 2007 Scanning holographic microscopy with resolution exceeding the Rayleigh limit of the objective by superposition of off-axis holograms *Appl. Opt.* **46** 993–1000
[26] Leith E, Chen C, Chen H, Chen Y, Dilworth D, Lopez J, Rudd J, Sun P-C, Valdmanis J and Vossler G 1992 Imaging through scattering media with holography *J. Opt. Soc. Am.* A **9** 1148–53
[27] Mills K, Zalevsky Z and Leith E N 2002 Holographic generalized first-arriving light approach for resolving images viewed through a scattering medium *Appl. Opt.* **41** 2116–21
[28] Zalevsky Z, Saat E, Orbach S, Mico V and Garcia J 2008 Exceeding the resolving imaging power using environmental conditions *Appl. Opt.* **47** A1–6
[29] Mico V, Zalevsky Z, García-Martínez P and García J 2006 Superresolved imaging in digital holography by superposition of tilted wavefronts *Appl. Opt.* **45** 822–8
[30] Mico V, Zalevsky Z and García J 2006 Superresolution optical system by common-path interferometry *Opt. Express* **14** 5168–77
[31] Price J R, Bingham P R and Thomas C E Jr 2007 Improving resolution in microscopic holography by computationally fusing multiple, obliquely illuminated object waves in the Fourier domain *Appl. Opt.* **46** 826–33
[32] Mico V, Zalevsky Z and García J 2007 Synthetic aperture microscopy using off-axis illumination and polarization coding *Opt. Commun.* **276** 209–17
[33] Mico V, Zalevsky Z and García J 2008 Common-path phase-shifting digital holographic microscopy: a way to quantitative imaging and superresolution *Opt. Commun.* **281** 4273–81
[34] Wilson T and Sheppard C J R 1984 *Theory and Practice of Scanning Optical Microscopy* (New York: Academic)
[35] Häusler G and Heckel W 1988 Light sectioning with large depth and high resolution *Appl. Opt.* **27** 5165–9
[36] Neil M A A, Juskaitis R and Wilson T 1997 Method of obtaining optical sectioning by using structured light in a conventional microscope *Opt. Lett.* **22** 1905–7
[37] Krzewina L G and Kim M K 2006 Single-exposure optical sectioning by color structured illumination microscopy *Opt. Lett.* **31** 477–9
[38] Engelbrecht Ch J and Stelzer E H K 2006 Resolution enhancement in a light-sheet-based microscope (SPIM) *Opt. Lett.* **31** 1477–9
[39] Poher V *et al* 2007 Optical sectioning microscopes with no moving parts using a micro-stripe array light emitting diode *Opt. Express* **15** 11196–206
[40] Voie A H, Burns D H and Spelman F A 1993 Orthogonal plane fluorescence optical sectioning: three-dimensional imaging of macroscopic biological specimen *J. Microsc.* **170** 229–36
[41] Stelzer E H K and Lindek S 1994 Fundamental reduction of the observation volume in far-field light microscopy by detection orthogonal to the illumination axis: confocal theta microscopy *Opt. Commun.* **111** 536–47
[42] Fuchs E, Jaffe J, Long R and Azam F 2002 Thin laser light sheet microscope for microbial oceanography *Opt. Express* **10** 145–54
[43] Huisken J, Swoger J, del Bene F, Wittbrodt J and Stelzer E H K 2004 Optical sectioning deep inside live embryos by selective plane illumination microscopy *Science* **305** 1007–9
[44] Verveer P J, Swoger J, Pampaloni F, Greger K, Marcello M and Stelzer E H K 2007 High-resolution three-dimensional imaging of large specimens with light sheet-based microscopy *Nat. Methods* **4** 311–3